Published in final edited form as:
Acta Biomater. 2013 January ; 9(1): 4787–4795. doi:10.1016/j.actbio.2012.08.021.

Elastic discontinuity due to ectopic calcification in a human fibrous joint

Jeremy D. Lin[1], **Shaul Aloni**[2], **Virginia Altoe**[2], **Samuel M. Webb**[3], **Mark I. Ryder**[4], and **Sunita P. Ho**[1]

[1]Division of Biomaterials and Bioengineering, Department of Preventive and Restorative Dental Sciences, University of California, San Francisco, San Francisco, CA

[2]The Molecular Foundry, Lawrence Berkeley National Laboratory, Berkeley, CA

[3]Stanford Synchrotron Radiation Lightsource, SLAC National Accelerator Laboratory, Menlo Park, CA

[4]Department of Orofacial Sciences, University of California, San Francisco, San Francisco, CA

Abstract

Disease can alter the natural ramp-like elastic gradients to steeper step-like profiles at soft-hard tissue interfaces. Prolonged function can further mediate mechanochemical events that alter biomechanical response within diseased organs. In this study a human bone-tooth fibrous joint was chosen as a model system, in which the effects of bacterial-induced disease, i.e. periodontitis, on natural elastic gradients were investigated. Specifically, the effects of ectopic biomineral, i.e. calculus, on innate chemical and elastic gradients within the diseased cementum-dentin complex in comparison to a healthy complex, both of which are fundamental parameters to load-bearing tissues, will be discussed.

Complementary techniques for mapping changes in physicochemical properties as a result of disease, included micro-X-ray computed tomography, microprobe micro X-ray fluorescence imaging, transmission electron and atomic force microscopy (TEM, AFM) techniques, and AFM-based nanoindentation. Results demonstrated primary effects as derivatives of ectopic mineralization within the diseased fibrous joint. Ectopic mineralization with no cementum resorption, but altered cementum physicochemical properties with increasing X-ray attenuation, exhibited stratified concretion with increasing X-ray fluorescence counts of calcium and phosphorus elements in the extracellular matrix. These were correlated to decreased hygroscopicity, indenter displacement, and apparent strain relieving characteristics. Disease progression identified as concretion through the periodontal ligament (PDL)-cementum enthesis and sometimes the originally hygroscopic cementum-dentin junction, resulted in a significantly increased indentation elastic modulus (3.16±1.19 GPa) and a shift toward a discontinuous interface compared to healthy conditions (1.54±0.83 GPa) (Student's *t*-test, $p<0.05$). The observed primary effects could result in secondary downstream effects, such as compromised mechanobiology at the mechanically active PDL-cementum enthesis that can catalyze disease progression.

To whom correspondence should be addressed: Sunita P. Ho, Ph.D., Division of Biomaterials and Bioengineering, Department of Preventive and Restorative Dental Sciences, University of California San Francisco, San Francisco, CA 94143, Phone: 415-514-2818.

1. INTRODUCTION

Interfaces exist in a multitude of living organisms and delineate dissimilar tissues (1, 2). Interestingly, these delineating interfaces under high spatial resolution most often illustrate a seamless integration that consists of a gradual transition from one tissue to another, indicating that the visibly discrete systems are indeed a continuum (2, 3). This fundamental characteristic of an interface is exploited in this study, in which any deviation from the naturally occurring elastic gradient is proposed as a “marker” of pathology. Furthermore, shifts in chemical and elastic gradients from a ramp-like to a step-like profile at interfaces could accelerate disease progression because of a secondary effect, i.e. compromised mechanobiology with prolonged function of a diseased joint.

Soft-hard tissue attachment sites (entheses) in the musculoskeletal and the oral and craniofacial systems are formed by insertions of soft, fibrous tendon/ligaments into mineralized tissues (4–7). This integration is due to structural rearrangement of collagen, interplay of water molecules with globular and fibrillar proteins, varying organic to inorganic ratios, and the nanosize crystal association within and around collagen fibrils. Such characteristics provide the load-bearing organ an optimum mechanical function throughout the life-span of an organism (6–10). Despite the seamless binding at the interface, mechanically loaded entheses experience higher strains simply because of significant differences in stiffness values between soft and hard tissues (11). These naturally highly strained attachment sites (12) can be compromised when compounded with external insults. Excessive loading and/or disease-induced perturbations locally may alter the load-bearing characteristics of the entheses. Within the musculoskeletal and oral and craniofacial systems, undesirable mineral advancement into adjacent organic matrices can occur due to aforementioned extrinsic factors. Mineralization of softer matrices at the entheses causes enthesophytes and/or osteophytes. The mineral formation alters joint mobility as a result of change in functional space (13, 14). Compared to most diarthroidal joints, the dento-alveolar organ is a fibrous joint with relatively less functional space (150–380 μm) and limited range of motion. Within this joint are several graded interfaces (functionally graded interfaces; FGI) that permit optimum function (6, 15, 16). However, compromised functional space due to bony protrusions or stratified bone growth were also identified as elastic discontinuities in the form of steeper modulus gradients at the periodontal ligament (PDL)-bone and PDL-cementum interfaces (3, 6) of the bone-tooth fibrous joint.

Two different mineralizing pathways that could occur at the soft-hard tissue attachment sites specific to bone-tooth fibrous joints are: 1) Biologically induced mineralization: the oral environment contains polymeric matrices of bacterial origin upon which calcium and phosphate ions in the supersaturated crevicular fluid deposit, resulting in ectopic mineralization (17); 2) Biologically controlled mineralization, also known as mechanobiology-based mineralization: cells at the strained soft-hard attachment sites regulate local biochemical signals within the extracellular matrix (ECM) (18). Subsequently, entheses adapt as a result of load-induced modeling: a form-function phenomenon that alters the biomechanical response of tissues and their attachment sites to match functional demands (19). We propose that both pathways could exist in a diseased yet functioning joint, and the resulting changes can be detected by mapping physicochemical parameters. Parameters include changes in microstructure, elemental composition, and ultimately the local load-resisting characteristics relative to healthy conditions. In this study we will map shifts in modulus profiles as a result of ectopic calcification of the cementum enthesis within a diseased human bone-tooth fibrous joint. A shift in modulus profile is proposed as an adaptive effect of the PDL-cementum and cementum-dentin interfaces due to globally prevalent and infectious periodontal disease.

Periodontitis is an oral disease characterized by host inflammatory responses that affect the load-bearing integrity of the attachment apparatus, eventually compromising function (20, 21). Patients with periodontitis often times have calculus formation (17, 22). This mineralized mass has a varied elemental composition (23–25) and unlike vascularized alveolar bone (AB), diseased avascularized cementum does not exhibit clinical resorption (26, 27). Diseased cementum was reported to contain higher calcium (Ca) and phosphorous (P) content at PDL-cementum entheses and interfacial regions than bulk cementum (28). Despite these observations, there is no information on how the adapted physicochemical properties of the cementum-dentin complex affect the natural gradients and biomechanical function of the tooth. We hypothesize that bacterial insult converts a functionally graded PDL-cementum interface into a discontinuous interface. The hypothesis was investigated by mapping physicochemical properties of diseased and healthy PDL-cementum and cementum-dentin complexes. Correlative high resolution imaging and spectroscopy were performed to underline the importance of natural gradients and, therefore, the strain- and stress-relieving attachment apparatus of a human bone-tooth complex.

2. MATERIALS AND METHODS

2.1. Ultrasectioned blocks for atomic force microscopy (AFM), nanoindentation, micro X-ray fluorescence (μ-XRF), and ultrasections for transmission electron microscopy (TEM)

Molars were obtained from humans requiring extractions as a part of dental treatment following a protocol approved by the UCSF Committee on Human Research. Roots from diseased and healthy molars from 40–60 year old males were gamma-radiated (29), longitudinally cut, and the resulting longitudinal halves containing primary cementum were transversely sectioned. Primary cementum also known as acellular cementum was identified by noting the absence of lacunae (30). The transverse sections were glued to AFM steel stubs (Ted Pella, Inc., Redding, CA) using ethyl α-cyanoacrylate (MDS Adhesive QX-4, MDS Products, Inc., Anaheim, CA). Specimens were then ultrasectioned using an Ultracut E ultramicrotome (Reichert Scientific Instrument Technical Services, Depew, NY) (31) and 60–90 nm thin sections were collected. Ultrathin sections were placed on carbon coated TEM grids for TEM analysis, while the relatively flat and orthogonal surface of the sectioned specimen block was used for AFM, AFM-based nanoindentation (31), and microprobe μ-XRF (3) analyses.

2.2. Histology

Healthy and diseased molars (N=3 each group) were fixed in 10% formalin (Lyne Laboratories, Inc., Soughton, MA) for two days, and decalcified using formic acid (Immunocal, Decal Chemical Corp., Tallman, NY) for two weeks. Following paraffin embedding, specimens were sectioned with a rotary microtome (Reichert-Jung Biocut, Vienna, Austria). 5–6 μm paraffin sections were mounted on Superfrost Plus microscope slides (Fisher Scientific, Fair Lawn, NJ), deparaffinized, and stained with picrosirius red (PSR). Stained sections were characterized with a light microscope (BX51, Olympus America, Inc., San Diego, CA). Polarized light was used to enhance collagen birefringence and resulting images were analyzed using Image Pro Plus v6.0 (Media Cybernetics, Inc., Silver Spring, MD).

2.3. Micro X-ray computed tomography (μ-XCT)

1×1 mm longitudinal beams containing cementum and dentin tissues were sectioned from healthy and diseased molars (N=3 each group) and polished with 1200 grit polishing paper. Macroscale structural analysis of the cementum-dentin complex was performed using μ-XCT (MicroXCT-200, Xradia, Inc., Pleasanton, CA) at 4× and 10× magnification under wet

conditions. X-ray imaging of specimens was performed using a tungsten anode with a setting of 70–75 KVp at 4 W.

2.4. Scanning electron microscope (SEM), AFM

For SEM analysis, molars (N=3 each group) were fixed in 10% formalin (Lyne Laboratories, Inc., Soughton, MA) for two days. Each molar was dehydrated before cryofracturing (6) and sputtered with a 100 nm gold-palladium coating (Hummer VII, Anatech Ltd. VA, USA). Specimens were then imaged at 5–10 keV using a S4300 SEM unit (Hitachi, Tokyo, Japan). Backscatter electron (BSE) imaging was performed at 15 keV. High-resolution qualitative microstructural analysis of the ultrasectioned cementum-dentin complex (N=5 each group; healthy and diseased) was performed under dry and wet conditions using a multimode AFM (Bruker, Santa Barbara, CA) (32).

2.5. Microprobe μ-XRF imaging

150 μm thick finely polished ground sections were imaged using a microprobe (Stanford Synchrotron Radiation Lightsource, Menlo Park, CA) μ-XRF technique. Images were acquired using an incident X-ray energy of 12 keV with a microfocused beam of 2 μm. Fluorescence lines of Ca and P were monitored using a beam exposure of 100 ms per pixel. Low resolution maps were generated with a scanning step size of 5 μm while high resolution maps were generated with scanning step size of 1 μm. All spectra and maps were analyzed using SMAK v0.51 (http://smak.sams-xrays.com/) (33).

2.6. Nanoindentation

Changes in indenter displacement into the healthy and diseased matrices by holding a peak load of 1500 μN over 3 seconds (32) provided site-specific displacement and apparent strain effects. Site-specific stiffness (S) and reduced elastic modulus (E_r) measurements were evaluated under wet conditions with the use of an AFM-based nanoindenter (Hysitron Inc., Minneapolis, MN) (32, 34, 35). S as predominantly determined by the load per unit deformation of organic, collagenous matrices was determined as the load-to-displacement ratio of the initial 30% of data in the unloading stage of a 3-stage load-hold-unload curve (35). The stiffness of organic, or predominantly organic, collagenous matrices is initially low owing to the natural crimps within collagen. A significant increase in load per unit deformation can only be observed once the crimps are removed and the fiber becomes taut. Hence, stiffness was mapped, while elastic modulus is an intrinsic and a constitutive property of the site-specific region being indented (36).

E_r was calculated based on the S value measured and the contact area of the indenter with the material (35). E_r was reported to determine if increased mineralization of the diseased complex affected the intrinsic molecular interactions within the tissues that form the enthesis. Changes in these interactions would alter intermolecular strains of diseased tissue structures in comparison to healthy structures.

Ultrasectioned blocks from diseased and healthy molars were used (N =3). Following a modified protocol (31), for each indent a maximum load of 1500 μN was used with load, hold, and unload times of 3 s each. Changes in indenter displacement into the healthy and diseased matrices (Fig. 5A) by holding a peak load of 1500 μN over 3 seconds (32) provided site-specific displacement and apparent viscoelastic strain effects. Fused silica was used as a standard to calibrate the transducer under both dry and wet conditions (6).

3. RESULTS

3.1. Calcified ectopic mass

3D tomography and 2D virtual sections of diseased roots illustrated higher X-ray attenuating patches along diseased cementum surfaces (Fig. 1d,f), and a lower X-ray attenuating zone indicative of the 100–200 μm interfacial zone between healthy cementum and dentin (31, 32) was observed under both healthy and diseased conditions (Fig. 1a–f). Rough surfaces due to ectopic calcification through a layer-by-layer mineral apposition that varied in X-ray attenuation (Fig. 1c,d) were observed on diseased root surfaces compared to healthy counterparts (Fig. 1a,b). Microscale regions of increased X-ray attenuation was noted within bulk cementum (Fig. 1e,f). Please see Supplemental Videos 1 and 2.

3.2. Ca and P elemental gradients

The diseased cementum enthesis exhibited a lighter gray color than that of the underlying bulk cementum (Fig. 2d), and healthy cementum (Fig. 2a). Contrary to the healthy complex, a semi-quantitative analysis indicated an increase in Ca and P elemental counts. Within the enthesis and bulk cementum regions, a 10% increase in Ca and a 33% increase in P were observed in diseased specimens compared to healthy specimens. Interestingly, the healthy complex demonstrated gradual transitions of Ca and P counts (Fig. 2b,c) from the root surface into dentin, contrasting the increase in Ca and P at the diseased enthesis (Fig. 2e,f).

3.3. Concretion of fibrous structures

Characteristic collagen fibril periodicity of 65–67 nm (37) within the healthy enthesis and bulk cementum (Fig. 3a,b) was observed. Furthermore, needle-like crystals were observed along collagen fibers (Fig. 3a,b, *insets*). Correlating diseased regions did not illustrate collagen fibril periodicity due to an increased density of crystals (Fig. 3c,d). Mineral deposits varied in size, were of a hexagonal shape (Fig. 3c,d) and exhibited interference fringes, demonstrating increased crystallinity at the diseased enthesis (Fig. 3c, *inset*) and within cementum (Fig. 3d, *inset*). Complementary data using polarized light, scanning electron and atomic force microscopy techniques illustrated loss in collagen birefringence, fibrous structure, and hygroscopicity at the diseased PDL-cementum enthesis, cementum, and at times the CDJ compared to healthy specimens (Fig. S1).

3.4. Shifts in reduced elastic modulus (E_r) gradients

A gradual increase in E_r from the cementum enthesis into root dentin was observed (Fig. 4a,c) (6). In contrast, the diseased complex exhibited altered E_r gradients from the enthesis into root dentin (Fig. 4b,c). The healthy and diseased CDJ had lower E_r values compared to dentin and cementum (Fig. 4a,b). In both healthy and diseased complexes, stiffness (S) values followed the same trends as described for E_r. A Student's *t*-test with a 95% confidence interval indicated a significant difference ($p<0.05$) in S and E_r between healthy and diseased entheses, cementum and CDJ (Fig. 4, *table*). Intra-regional comparisons within the healthy complex showed a significant difference between the enthesis and bulk cementum ($p<0.05$) but not between the enthesis and CDJ. In contrast, the diseased complex showed no significant difference between the enthesis and bulk cementum but a significant difference between the enthesis and CDJ ($p<0.05$).

3.5. Displacement at peak indentation load

Under wet conditions, decreased indenter displacement during the hold phase (Fig. 5a) at the diseased compared to the healthy enthesis (Fig. 5b) was observed. Furthermore, the change in peak load over the same time for diseased enthesis was lower than for healthy enthesis (Fig. 5c).

4. DISCUSSION

Based on the results from this study, we propose that ectopic mineral, i.e. “biologically induced mineralization,” can compromise “biologically controlled mineralization”. Moreover, a combination of the two can accelerate disease progression under prolonged function. Biologically induced mineralization includes ectopic calcified masses (17, 38), such as calculus, atherosclerotic plaque, gallstones, calcified tumors, and kidney stones (39–41). In this study, as a result of calcified mass adjacent to cementum, we identified increased mineral density variations (Figs. 1 and 2), concretion of collagen fibers (Figs. 3 and S1), and shifts in modulus gradients (Fig. 4), including decreased indenter displacement and apparent strain relieving characteristics (Fig. 5) at the PDL-cementum and cementum-dentin interfaces. The correlative physicochemical mapping provided insights to propose a downstream secondary effect that could include unfavorable cell-mediated mineral formation and/or resorption related events, thus accelerating disease progression (Fig. 6).

Inception of layer-by-layer ectopic biomineral mass occurs from organic matrices with monomeric basic constituents at solid-liquid and liquid-air interfaces in supersaturated solutions. At solid-liquid interfaces, such as those found within a bone-tooth complex, an adhesive layer consisting of many organic constituents, such as polysaccharides, proteins, and glycolipids, creates a polymeric niche and a surface with high affinity to bacterial pathogens and their sessility (42). The long-term site-specific harboring of such bacteria on the slimy plaque layer triggers a cascade of destructive inflammatory events, including enzymatic degradation of nucleation inhibitors that maintain the supersaturation of gingival crevicular fluid, thus inducing mineralization pathways adjacent to the cementum surface. As a result, local rises in concentrations of calcium and phosphate ions and rises in plaque pH to alkaline levels cause nucleation of calcium phosphate salts on plaque (43). Additionally, bacteria within the plaque create intercellular alkaline regions that act as nucleators for subsequent biomineralization. In such a case, the matrix between the micro-organisms becomes calcified, and eventually mineralizes the bacteria (38, 39). Over time, the mineral phase, extent of mineralization, and type of mineral changes with disease progression (17, 44), thus increasing the overall mineral content. These events provide a stratified appearance as indicated by higher and lower X-ray attenuating layers (Fig. 1c–f).

Increased mineralization of cementum surface layers is sometimes observed in diseased specimens without calculus, and could be initiated through mechanisms similar to those seen in calculus formation. These mechanisms include bacterial-induced processes and/or diffusion and nucleation of inorganic calcium and phosphate ions on the exposed organic-rich enthesial ligaments. Results indicating higher attenuating mineral on the cementum surface and within subsurface layers of cementum (Figs. 1c–f and 2e,f) are in agreement with others (28, 44, 45). These layers illustrated dominance of higher atomic number elements (Fig. 2) of Ca and P within the affected enthesis and cementum and towards the hygroscopic CDJ (Fig. 2b,c,e,f). At the enthesis, it is conceivable that the PDL radial-inserts act as “wicks”, which permit an influx of Ca and P ions that could promote mineralization of the predominantly organic fibrous structures within cementum and at the cementum-dentin interface. Hence, the soft-hard, PDL-cementum hygroscopic attachment site and the hard-hard, cementum-dentin interface that both run apically down the roots are proposed to act as paths of least resistance and could permit concretion of collagen fibers.

Compromising of the functional integrity of the enthesis and organic-rich regions in cementum begins with an offset in the homeostatic repair mechanism through proteases as a response to disease (46, 47). Hence, the biochemical breakdown of a collagen molecular structure could result in a decrease in collagen birefringence (Fig. S1d) (48) and loss in fiber orientation and collagen periodicity (Figs. 3 and S1e,f). The added effect of loss in collagen

structure and deposition of mineral extrinsic to collagen fibrils decreased the visibility of collagen fibril periodicity (Fig. 3c,d) and hygroscopicity (Fig. 4b) (3, 6, 49), which are all significant characteristics of the affected enthesis and cementum-dentin complex. Concretion of collagen fibers at the enthesis and within cementum can be further corroborated by the increased and varied mineral deposits, crystal maturation, and altered crystal shapes and sizes, at the diseased enthesis (Figs. 2 and 3) (17, 50–53). These unwanted characteristics shifted the graded ramp-like E_r profile to a steeper step-like modulus profile at the PDL-cementum interface (Figs. 2 and 4).

Key basic constituents responsible for a functional soft-hard tissue interface should include intact collagen fibrils consisting of intra- and extra-fibrillar mineral deposits (54, 55). Additionally, the polyanionic proteoglycans (PGs) are responsible for structure and water retention of entheses and interfacing tissues. PGs covalently interact with collagen fibrils (56, 57), play a fundamental role in maintaining functional integrity, and are abundantly found at the healthy fibrous enthesis and CDJ (6). In addition to intrafibrillar water interactions within the collagen fibril, PGs increase the hygroscopicity of tissues and interfaces and contribute to matrix swelling (58, 59).

Hygroscopicity of interfaces predominantly at the mechanically strained soft-hard tissue attachment sites is essential (5, 6, 60, 61). The effect of enthesial hygroscopicity was best demonstrated by decreased local deformations at the diseased entheses and cementum in response to static load over time relative to healthy conditions (Fig. 5b,c). Decreased displacement at the diseased enthesis (Fig. 5b) indicated decreased strain relieving (shape memory) characteristics (Fig. 5b,c). Structures identified through collagen fibrils and extrafibrillar PGs, which together with bound water and intra- and extra-fibrillar mineral interactions, dissipate strain buildup via delayed movement within a tissue (61). These combined for decreased displacement effects over time, including: 1) the aforementioned loss in structure of the water-retentive collagen-PG network due to proteolytic fragmentation and/or defibrillation of organic collagen fibrils (5, 61, 62), and 2) increased concretion of the normally organic-rich PDL inserts (28, 45, 49). Given such a scenario, it is likely that the recoil energy of collagen and organic-rich regions at the interfaces within a tooth (enthesis and cementum-dentin complex) is decreased (63, 64).

The significant increase in E_r of the affected regions complements altered intrinsic molecular interactions within the tissues that form the enthesis. As a result, the diseased complex exhibited step-wise E_r and S profiles (Fig. 4b) similar to the chemical profiles of Ca and P (Fig. 2e,f). Interestingly, the extent of overlap in E_r and S values between diseased and healthy specimens illustrated the degree of disease and that the enthesis is similar in mechanical characteristics to the diseased cementum and CDJ (Fig. 5d). This implies that decreased displacement existed in the diseased enthesis as compared to the healthy enthesis. Hence, apparent strain relieving characteristics of the once heterogeneous enthesis, bulk cementum, and CDJ, could eventually act as a single homogenous tissue upon calcification with a loss in functionally graded characteristics and increased E_r and S. Moreover, transitions in E_r between cementum (1–8 GPa, *wet conditions*) and the relatively more mineralized dentin (10–25 GPa, *wet conditions*) could compromise tooth mechanics, affecting the overall bone-tooth biomechanics. Interestingly, despite severe diseased conditions, the significant overlap of S and E_r values between healthy and diseased bulk cementum (Fig. 5e) illustrates the potential for regenerative attachment to restore functionally graded interfaces, while those that fall outside of the healthy range may have been altered beyond their regenerative potential.

In summary, the following model is proposed, illustrating two integrated mechanisms that drive the progression of periodontitis through 1) ectopic calcification and 2) compromised

mechanobiology (Fig. 6). Under healthy conditions, stiffness gradients at PDL-AB and PDL-cementum interfaces relieve function-induced strains (Fig. 6a, 6b) (6, 12). Periodontitis is known to cause increased range of motion of the tooth due to loss of coronal periodontal support (Fig. 6c). Based on our results, the bacterial insult causes concretion of the PDL-cementum enthesis, shifting modulus gradients at the interface (Fig. 6d) (E_r profiles from ramp-like to step-like across the PDL-cementum interface). These events could cause compromised mechanotransduction, eliciting mineralization and/or resorption effects (3, 18, 65–68) and further altering the overall biomechanics of the bone-PDL-tooth complex. Hence it is plausible that a combinatorial effect of the aforementioned mechanisms upon prolonged function can create a perpetuating self-degrading mechanism.

5. CONCLUSION

This study examines how ectopic calcified mass in the periodontium can alter the PDL-cementum FGI and subsequently the overall biomechanical function of a bone-tooth complex. The PDL-cementum-dentin complex is an excellent model in describing this phenomenon as it contains remarkable graded properties and is susceptible to degeneration as a result of calculus formation and inflammatory response. Combined physicochemical markers for a compromised PDL-cementum-dentin complex include collagen fibril/fiber degradation, increases in Ca and P contents indicating hypermineralization, loss of hygroscopicity, and loss of much needed strain-relieving characteristics at the enthesis and CDJ. These changes in physicochemical properties were correlated to increased stiffness gradients of the fibrous joints. The shifts in E_r profiles could result in discontinuities with progression of disease and compromise the overall biomechanics of the bone-tooth organ. Future spatiotemporal studies via animal models would specifically identify the aforementioned cascade of events that simultaneously drive the degradation of the organic tissue and altered mineral content of the cementum surface in a systematic fashion. Furthermore, animal studies would allow mapping spatiotemporal adaptation of the entire bone-tooth complex as it is difficult to acquire pristine bone and PDL specimens from humans.

Supplementary Material

Refer to Web version on PubMed Central for supplementary material.

Acknowledgments

The authors thank Dr. Jim De Yoreo, Molecular Foundry, LBNL, CA and Dr. Arthur Veis, Northwestern University Medical School, IL for the many insightful discussions. Microprobe μ-XRF imaging was performed at the Stanford Synchrotron Radiation Lightsource (SSRL), SLAC National Accelerator Laboratory, Stanford University, CA. The authors also like to thank Lawrence Berkeley National Laboratories, for the use of SEM and BSE, and Dr. Peter Sargent, Ph.D., Department of Cell and Tissue Biology, UCSF, for the use of the ultramicrotome. Support was provided by NIH/NIDCR R00DE018212, NIH/NIDCR R01DE022032, NIH/NIDCR T32 DE07306, NIH/NCRR S10RR026645, and Departments of Preventive and Restorative Dental Sciences and Orofacial Sciences, UCSF.

REFERENCES

1. Dunlop JWC, Weinkamer R, Fratzl P. Artful interfaces within biological materials. Materials Today. 2011; 14(3):70–78.
2. Thompson, DAW. On growth and form. An abridged ed.. , editor. Cambridge Eng.: University Press; 1961.
3. Hurng JM, Kurylo MP, Marshall GW, Webb SM, Ryder MI, Ho SP. Discontinuities in the human bone-PDL-cementum complex. Biomaterials. 2011; 32(29):7106–7117. [PubMed: 21774982]

4. Benjamin M, Kumai T, Milz S, Boszczyk BM, Boszczyk AA, Ralphs JR. The skeletal attachment of tendons—tendon ‘entheses’. Comparative Biochemistry and Physiology - Part A: Molecular &amp. Integrative Physiology. 2002; 133(4):931–945.
5. Ho SP, Marshall SJ, Ryder MI, Marshall GW. The tooth attachment mechanism defined by structure, chemical composition and mechanical properties of collagen fibers in the periodontium. Biomaterials. 2007; 28(35):5238–5245. [PubMed: 17870156]
6. Ho SP, Kurylo MP, Fong TK, Lee SS, Wagner HD, Ryder MI, et al. The biomechanical characteristics of the bone-periodontal ligament-cementum complex. Biomaterials. 2010; 31(25): 6635–6646. [PubMed: 20541802]
7. Herring, SW. Biomechanics of teeth in bone: function, movement, and prosthetic rehabilitation. In: McCauley, LK.; Somerman, MJ., editors. Mineralized Tissues in Oral and Craniofacial Sceince Biological Principles and Clincal Correlates. 1 ed. A John Wiley & Sons Inc.; 2012. p. 255
8. Fong H, Sarikaya M, White SN, Snead ML. Nano-mechanical properties profiles across dentin–enamel junction of human incisor teeth. Materials Science and Engineering: C. 2000; 7(2):119–128.
9. Marshall GW Jr, Balooch M, Gallagher RR, Gansky SA, Marshall SJ. Mechanical properties of the dentinoenamel junction: AFM studies of nanohardness, elastic modulus, and fracture. Journal of biomedical materials research. 2001; 54(1):87–95. [PubMed: 11077406]
10. Benjamin M, Toumi H, Ralphs JR, Bydder G, Best TM, Milz S. Where tendons and ligaments meet bone: attachment sites ('entheses') in relation to exercise and/or mechanical load. Journal of anatomy. 2006; 208(4):471–490. [PubMed: 16637873]
11. Suresh S. Graded materials for resistance to contact deformation and damage. Science. 2001; 292(5526):2447–2451. [PubMed: 11431558]
12. Qian L, Todo M, Morita Y, Matsushita Y, Koyano K. Deformation analysis of the periodontium considering the viscoelasticity of the periodontal ligament. Dental materials : official publication of the Academy of Dental Materials. 2009; 25(10):1285–1292. [PubMed: 19560807]
13. Rogers J, Shepstone L, Dieppe P. Bone formers: osteophyte and enthesophyte formation are positively associated. Annals of the rheumatic diseases. 1997; 56(2):85–90. [PubMed: 9068279]
14. Shaw HM, Benjamin M. Structure-function relationships of entheses in relation to mechanical load and exercise. Scandinavian journal of medicine & science in sports. 2007; 17(4):303–315. [PubMed: 17490450]
15. Marshall SJ, Balooch M, Habelitz S, Balooch G, Gallagher R, Marshall GW. The dentin–enamel junction—a natural, multilevel interface. Journal of the European Ceramic Society. 2003; 23(15): 2897–2904.
16. Zaslansky P, Friesem AA, Weiner S. Structure and mechanical properties of the soft zone separating bulk dentin and enamel in crowns of human teeth: insight into tooth function. Journal of structural biology. 2006; 153(2):188–199. [PubMed: 16414277]
17. White DJ. Dental calculus: recent insights into occurrence, formation, prevention, removal and oral health effects of supragingival and subgingival deposits. European journal of oral sciences. 1997; 105(5 Pt 2):508–522. [PubMed: 9395117]
18. Krishnan V, Davidovitch Z. Cellular, molecular, and tissue-level reactions to orthodontic force. American journal of orthodontics and dentofacial orthopedics : official publication of the American Association of Orthodontists, its constituent societies, and the American Board of Orthodontics. 2006; 129(4):469 e1–469 e32.
19. Sun Z, Lee E, Herring SW. Cranial sutures and bones: growth and fusion in relation to masticatory strain. The anatomical record Part A, Discoveries in molecular, cellular, and evolutionary biology. 2004; 276(2):150–161.
20. Bascones-Martinez A, Figuero-Ruiz E. Periodontal diseases as bacterial infection. Medicina oral, patologia oral y cirugia bucal. 2004; 9(Suppl):101–107. 92-0.
21. Scannapieco FA. Periodontal inflammation: from gingivitis to systemic disease? Compend Contin Educ Dent. 2004; 25(Suppl 1)(7):16–25. [PubMed: 15645883]
22. Satheesh K, MacNeill SR, Rapley JW, Cobb CM. The CEJ: a biofilm and calculus trap. Compend Contin Educ Dent. 2011; 32(2):30, 2–7. [PubMed: 21473298]

23. Jin Y, Yip HK. Supragingival calculus: formation and control. Critical reviews in oral biology and medicine : an official publication of the American Association of Oral Biologists. 2002; 13(5): 426–441. [PubMed: 12393761]
24. Tsuda H, Arends J. Raman spectra of human dental calculus. Journal of dental research. 1993; 72(12):1609–1613. [PubMed: 8254131]
25. Little MF, Hazen SP. Dental Calculus Composition. 2. Subgingival Calculus: Ash, Calcium, Phosphorus, and Sodium. Journal of dental research. 1964; 43:645–651. [PubMed: 14197048]
26. Nanci A, Bosshardt DD. Structure of periodontal tissues in health and disease. Periodontology 2000. 2006; 40:11–28. [PubMed: 16398683]
27. Nociti FH Jr, Foster BL, Barros SP, Darveau RP, Somerman MJ. Cementoblast gene expression is regulated by Porphyromonas gingivalis lipopolysaccharide partially via toll-like receptor-4/MD-2. Journal of dental research. 2004; 83(8):602–607. [PubMed: 15271967]
28. Selvig KA, Hals E. Periodontally diseased cementum studied by correlated microradiography, electron probe analysis and electron microscopy. Journal of periodontal research. 1977; 12(6): 419–429. [PubMed: 145479]
29. Brauer DS, Saeki K, Hilton JF, Marshall GW, Marshall SJ. Effect of sterilization by gamma radiation on nano-mechanical properties of teeth. Dental materials : official publication of the Academy of Dental Materials. 2008; 24(8):1137–1140. [PubMed: 18436298]
30. Foster, BL.; Somerman, MJ. Cementum. In: McCauley, LK.; Somerman, MJ., editors. Mineralized Tissues in Oral and Craniofacial Sceince Biological Principles and Clincal Correlates. 1 ed. A John Wiley & Sons Inc.; 2012. p. 169-170.
31. Ho SP, Goodis H, Balooch M, Nonomura G, Marshall SJ, Marshall G. The effect of sample preparation technique on determination of structure and nanomechanical properties of human cementum hard tissue. Biomaterials. 2004; 25(19):4847–4857. [PubMed: 15120532]
32. Ho SP, Balooch M, Marshall SJ, Marshall GW. Local properties of a functionally graded interphase between cementum and dentin. Journal of biomedical materials research Part A. 2004; 70(3):480–489. [PubMed: 15293322]
33. Webb SM. The Microanalysis Toolkit: X-ray fluorescence image processing software. AIP Conf Proc. 2011; 1365:196–199.
34. Van Landingham, MR.; Villarrubia, JS.; Guthrie, WF.; Meyers, GF., editors. Macromolecular symposia : Advances in scanning probe microscopy of polymers. New York: John Wiley & Sons; 2001. Nanoindentation of polymers: An overview.
35. Pharr GM, Oliver WC, Brotzen FR. On the Generality of the Relationship among Contact Stiffness, Contact Area, and Elastic-Modulus during Indentation. J Mater Res. 1992; 7(3):613–617.
36. Gere, JM.; Timoshenko, SP. Mechanics of Materials, Axially loaded members. Boston Masschusetts: PWS Publishers; 1984. p. 49
37. Paige MF, Rainey JK, Goh MC. A study of fibrous long spacing collagen ultrastructure and assembly by atomic force microscopy. Micron. 2001; 32(3):341–353. [PubMed: 11006515]
38. Carranza, FA.; Newman, MG. Clinical Periodontology. 8th ed. W.B. Saunders Company; 1996.
39. Demir T. Is there any relation of nanobacteria with periodontal diseases? Medical hypotheses. 2008; 70(1):36–39. [PubMed: 17587506]
40. Zhang SM, Tian F, Jiang XQ, Li J, Xu C, Guo XK, et al. Evidence for calcifying nanoparticles in gingival crevicular fluid and dental calculus in periodontitis. Journal of periodontology. 2009; 80(9):1462–1470. [PubMed: 19722797]
41. Kajander EO, Ciftcioglu N. Nanobacteria: an alternative mechanism for pathogenic intra- and extracellular calcification and stone formation. Proceedings of the National Academy of Sciences of the United States of America. 1998; 95(14):8274–8279. [PubMed: 9653177]
42. Davey ME, O'Toole GA. Microbial biofilms: from ecology to molecular genetics. Microbiology and molecular biology reviews : MMBR. 2000; 64(4):847–867. [PubMed: 11104821]
43. Sikes, CS.; Wheeler, AP. American Chemical Society. Division of Industrial and Engineering Chemistry., American Chemical Society. Meeting. Surface reactive peptides and polymers : discovery and commercialization : developed from a symposium sponsored by the Division of

Industrial and Engineering Chemistry at the 197th National Meeting of the American Chemical Society; April 12–13, 1989; Dallas, Texas. Washington, DC: The Society; 1991.

44. Nancollas GH, Johnsson MA. Calculus formation and inhibition. Advances in dental research. 1994; 8(2):307–311. [PubMed: 7865091]
45. Bosshardt DD, Selvig KA. Dental cementum: the dynamic tissue covering of the root. Periodontology 2000. 1997; 13(1):41–75. [PubMed: 9567923]
46. Hernandez M, Dutzan N, Garcia-Sesnich J, Abusleme L, Dezerega A, Silva N, et al. Host-pathogen interactions in progressive chronic periodontitis. Journal of dental research. 2011; 90(10):1164–1170. [PubMed: 21471325]
47. Sorsa T, Tjaderhane L, Konttinen YT, Lauhio A, Salo T, Lee HM, et al. Matrix metalloproteinases: contribution to pathogenesis, diagnosis and treatment of periodontal inflammation. Annals of medicine. 2006; 38(5):306–321. [PubMed: 16938801]
48. Junqueira LC, Bignolas G, Brentani RR. Picrosirius staining plus polarization microscopy, a specific method for collagen detection in tissue sections. The Histochemical journal. 1979; 11(4): 447–455. [PubMed: 91593]
49. Bilgin E, Gurgan CA, Arpak MN, Bostanci HS, Guven K. Morphological changes in diseased cementum layers: a scanning electron microscopy study. Calcified tissue international. 2004; 74(5):476–485. [PubMed: 14994104]
50. Tohda H, Fejerskov O, Yanagisawa T. Transmission electron microscopy of cementum crystals correlated with Ca and F distribution in normal and carious human root surfaces. Journal of dental research. 1996; 75(3):949–954. [PubMed: 8675807]
51. Orban, BJ.; Bhaskar, SN. Orban's oral histology and embryology. 11th ed.. St. Louis: Mosby Year Book; 1991.
52. Roberts-Harry EA, Clerehugh V. Subgingival calculus: where are we now? A comparative review. Journal of dentistry. 2000; 28(2):93–102. [PubMed: 10666966]
53. Lagier R, Baud CA. Magnesium whitlockite, a calcium phosphate crystal of special interest in pathology. Pathology, research and practice. 2003; 199(5):329–335.
54. Bertassoni LE, Habelitz S, Marshall SJ, Marshall GW. Mechanical recovery of dentin following remineralization in vitro--an indentation study. Journal of biomechanics. 2011; 44(1):176–181. [PubMed: 20926080]
55. Balooch M, Habelitz S, Kinney JH, Marshall SJ, Marshall GW. Mechanical properties of mineralized collagen fibrils as influenced by demineralization. Journal of structural biology. 2008; 162(3):404–410. [PubMed: 18467127]
56. Scott JE. Proteoglycan-fibrillar collagen interactions. The Biochemical journal. 1988; 252(2):313–323. [PubMed: 3046606]
57. Seog J, Dean D, Plaas AHK, Wong-Palms S, Grodzinsky AJ, Ortiz C. Direct Measurement of Glycosaminoglycan Intermolecular Interactions via High-Resolution Force Spectroscopy. Macromolecules. 2002; 35(14):5601–5615.
58. Maroudas A. Biophysical chemistry of cartilaginous tissues with special reference to solute and fluid transport. Biorheology. 1975; 12(3–4):233–248. [PubMed: 1106795]
59. Maroudas AI. Balance between swelling pressure and collagen tension in normal and degenerate cartilage. Nature. 1976; 260(5554):808–809. [PubMed: 1264261]
60. Ho SP, Balooch M, Goodis HE, Marshall GW, Marshall SJ. Ultrastructure and nanomechanical properties of cementum dentin junction. Journal of biomedical materials research Part A. 2004; 68(2):343–351. [PubMed: 14704976]
61. Ho SP, Sulyanto RM, Marshall SJ, Marshall GW. The cementum-dentin junction also contains glycosaminoglycans and collagen fibrils. Journal of structural biology. 2005; 151(1):69–78. [PubMed: 15964205]
62. Selvig KA. Ultrastructural changes in cementum and adjacent connective tissue in periodontal disease. Acta Odontologica Scandinavica. 1966; 24(4):459–500.
63. Landis WJ. A study of calcification in the leg tendons from the domestic turkey. Journal of ultrastructure and molecular structure research. 1986; 94(3):217–238. [PubMed: 3027205]
64. Landis WJ, Librizzi JJ, Dunn MG, Silver FH. A study of the relationship between mineral content and mechanical properties of turkey gastrocnemius tendon. Journal of bone and mineral research :

the official journal of the American Society for Bone and Mineral Research. 1995; 10(6):859–867. [PubMed: 7572309]

65. Ingber DE. Mechanobiology and diseases of mechanotransduction. Annals of medicine. 2003; 35:564–577. [PubMed: 14708967]
66. Ingber DE. Tissue adaptation to mechanical forces in healthy, injured and aging tissues. Scandinavian journal of medicine & science in sports. 2005; 15:199–201. [PubMed: 15998336]
67. Ingber DE. Cellular mechanotransduction: putting all the pieces together again. The FASEB journal : official publication of the Federation of American Societies for Experimental Biology. 2006; 20:811–827.
68. Wang N, Tytell JD, Ingber DE. Mechanostransduction at a distance: mechanically coupling the extracellular matrix with the nucleus. Nature Reviews, Molecular Cell Biology. 2009; 10:75–82.

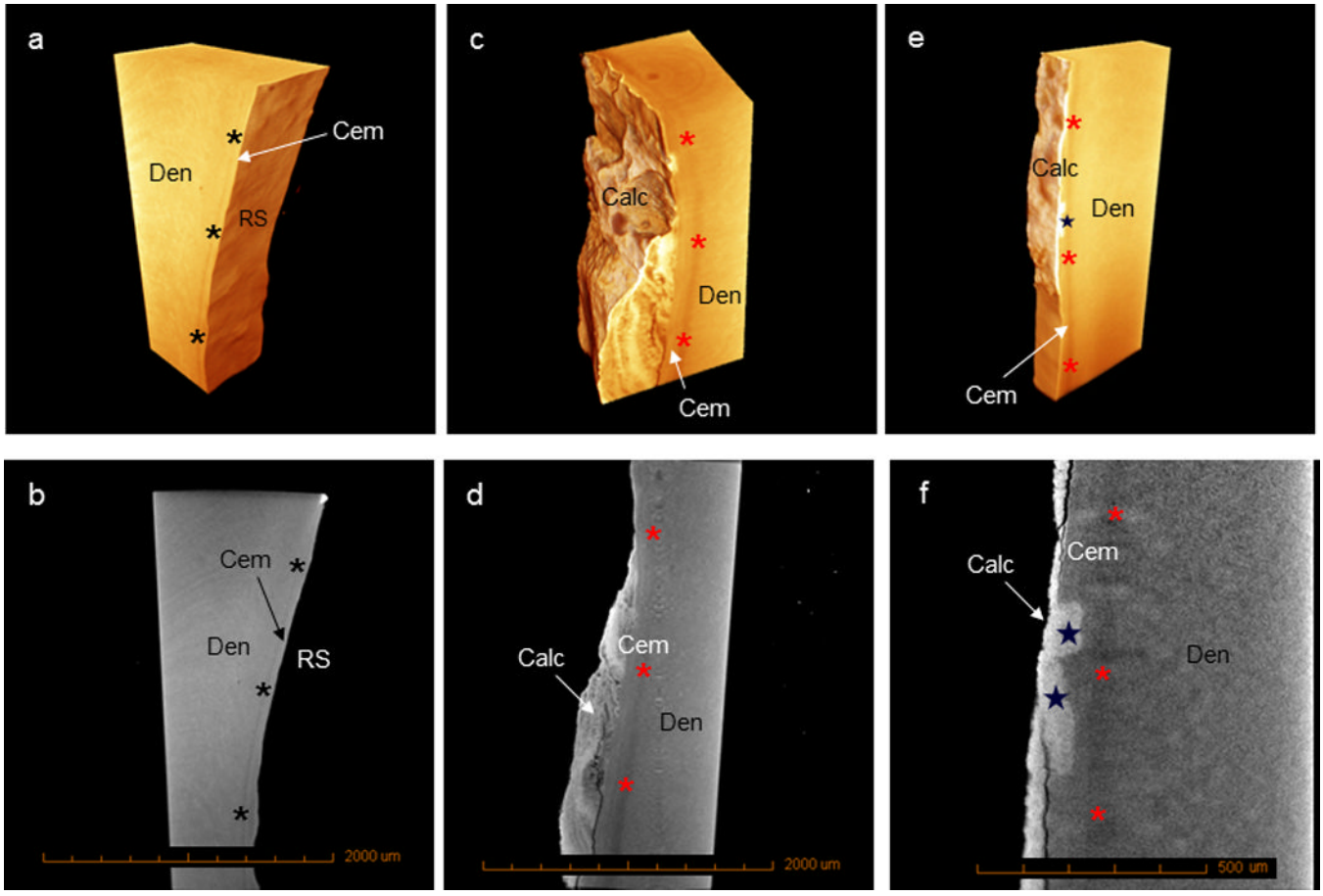

Figure 1.

3D tomographs and virtual sections reveal a transitional hypomineralized zone between cementum and dentin under healthy (a, b, black asterisks) and diseased (c–f, red asterisks) conditions. Healthy root surfaces lack ectopic calcified mass (a, b), while diseased root surfaces contain a calcified mass (c–f). Calculus can be identified as higher X-ray attenuating regions (c–f) with or without lamellar structures (c, d). Increasing mineral buildup in bulk cementum (e, f, stars) can also be seen under diseased conditions. (Calc – calculus; Cem – cementum; Den – dentin; RS – root surface)

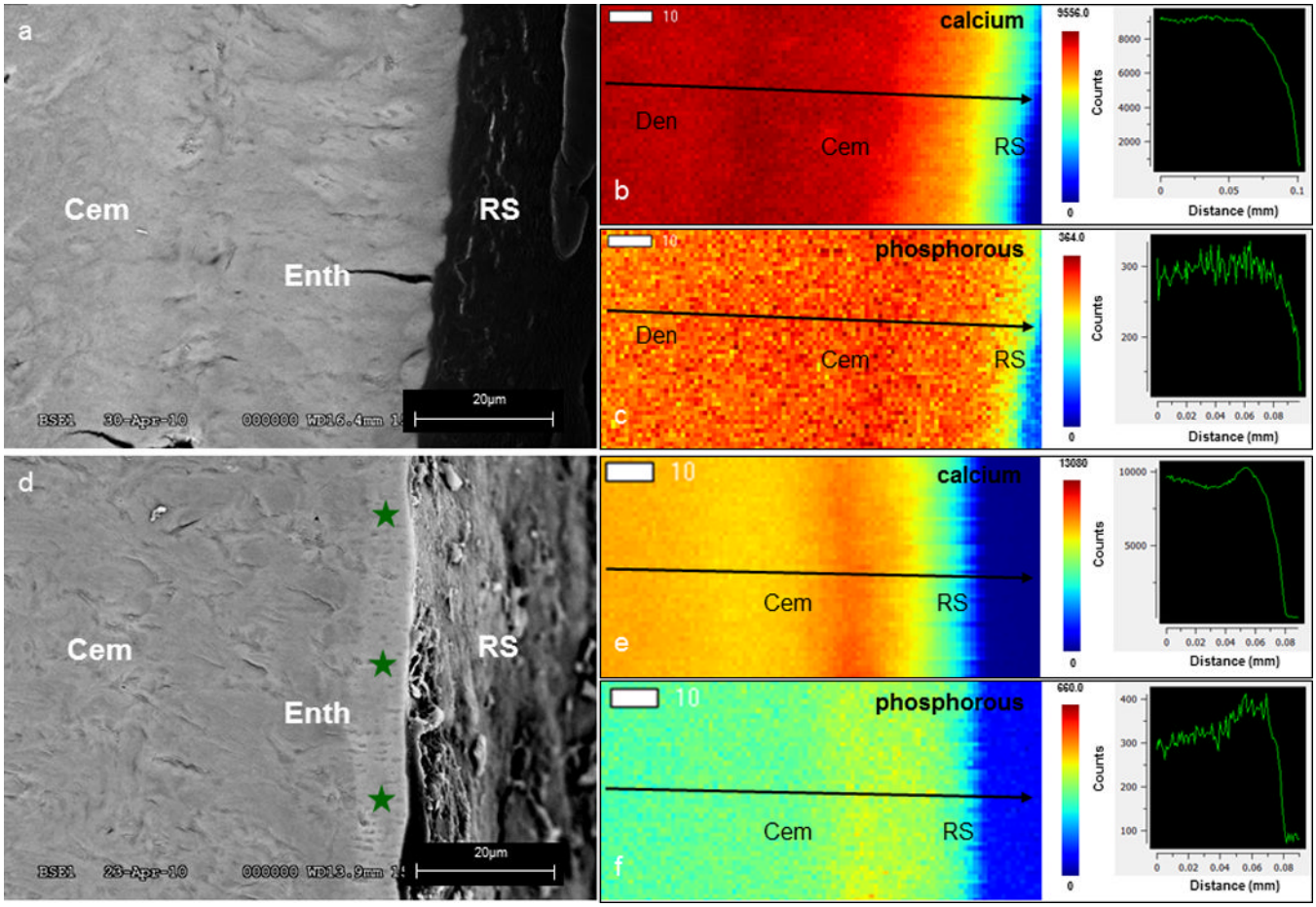

Figure 2.

Backscatter scanning electron microscopy (a, d) illustrates grey scale differences between the superficial cementum layer and bulk cementum of healthy (a) and diseased (d, green stars) cementum-dentin complexes. μ-XRF maps of Ca and P elements (b, c, e, f) show site-specific variations in counts. Line profiles (arrows) illustrate gradients of Ca and P counts in the healthy complex (b, c) and an altered Ca and P gradient through the diseased complex (e, f). (Cem – cementum; Den – dentin; RS – root surface)

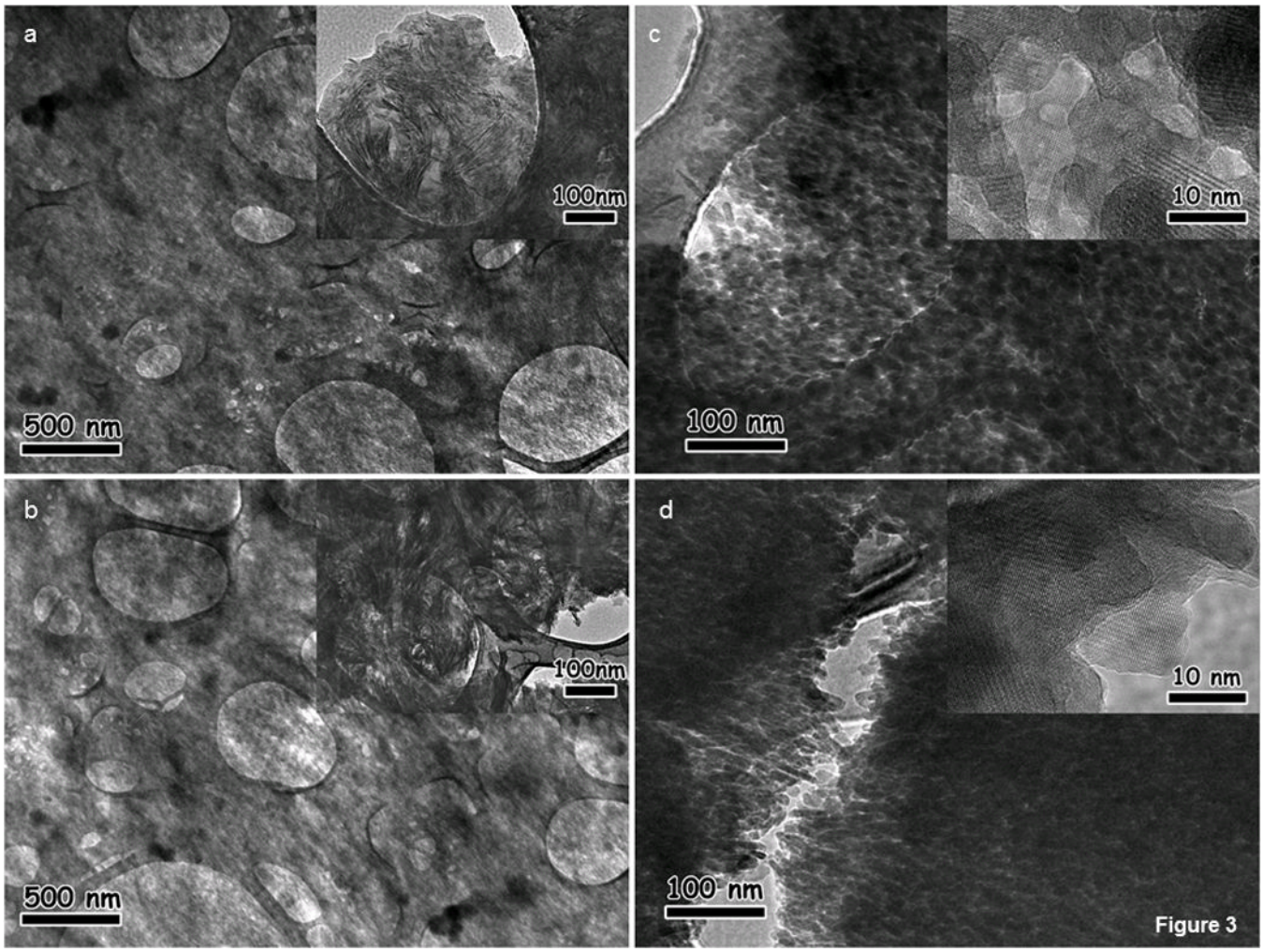

Figure 3.
TEM illustrates collagen fibrils at the healthy cementum enthesis (a) and in cementum (b). Higher magnification reveals needle-like mineral deposits (insets, a, b) in the healthy enthesis and cementum. The diseased enthesis (c) and cementum (d) exhibits increased density and different sizes and shapes of mineral deposits. Higher magnification of diseased regions illustrates individual crystals that present lattice fringes (insets, c, d).

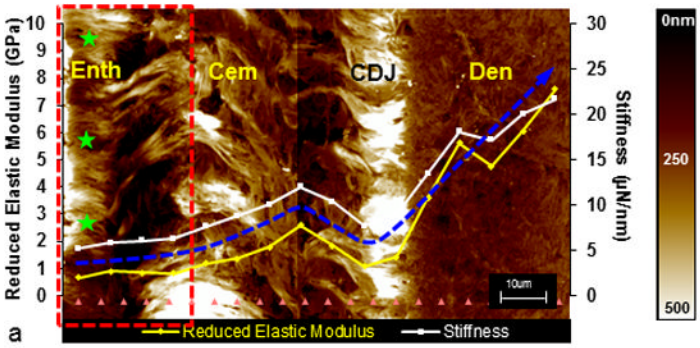

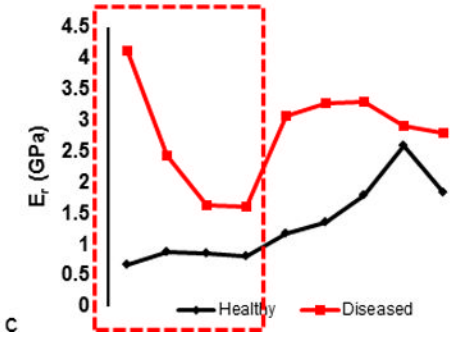

Reduced Elastic Modulus (GPa)				
Condition	**Enthesis**	**Cementum**	**CDJ**	**Dentin**
Healthy	1.54 ± 0.83[a,c]	2.93 ± 1.45[c]	1.29 ± 0.27[g]	7.93 ± 2.47
Diseased	3.16 ± 1.19[a,e]	2.96 ± 1.66	1.93 ± 0.78[g,e]	6.81 ± 3.62
Stiffness (μN/nm)				
Condition	**Enthesis**	**Cementum**	**CDJ**	**Dentin**
Healthy	8.74 ± 3.19[b,d]	12.17 ± 2.98[d]	8.29 ± 0.59[h]	19.59 ± 5.40
Diseased	11.52 ± 2.75[b,f]	11.17 ± 3.78	9.73 ± 2.61[h,f]	15.88 ± 5.56

Note: [a,b,c,d,e,f,g,h] *indicate relevant significant differences*

Figure 4.

Wet AFM micrographs illustrate hydration of the healthy enthesis (a, green stars) compared to minimal hydration of the diseased enthesis (b, teal stars). Arrays of indents (a, b, pink triangles) illustrate the nanoindentation scheme through ultrasectioned block surfaces of both diseased and healthy cementum-dentin complexes. E_r and S line profiles from root surface into dentin reveal a loss in stiffness graded properties in diseased specimens compared to a gradual gradient in healthy specimens. Blue and green arrows are representative E_r profiles for healthy and diseased conditions, respectively. E_r alone for healthy (c, black) and diseased (c, red) enthesis regions (a–c, red boxes) are plotted. Table illustrates average E_r and S values of specific regions within the complex under healthy and diseased conditions. Significant differences in E_r and S between healthy and diseased regions are marked (superscripts). (Enth – enthesis; Cem – cementum; CDJ – cementum-dentin junction; Den – dentin)

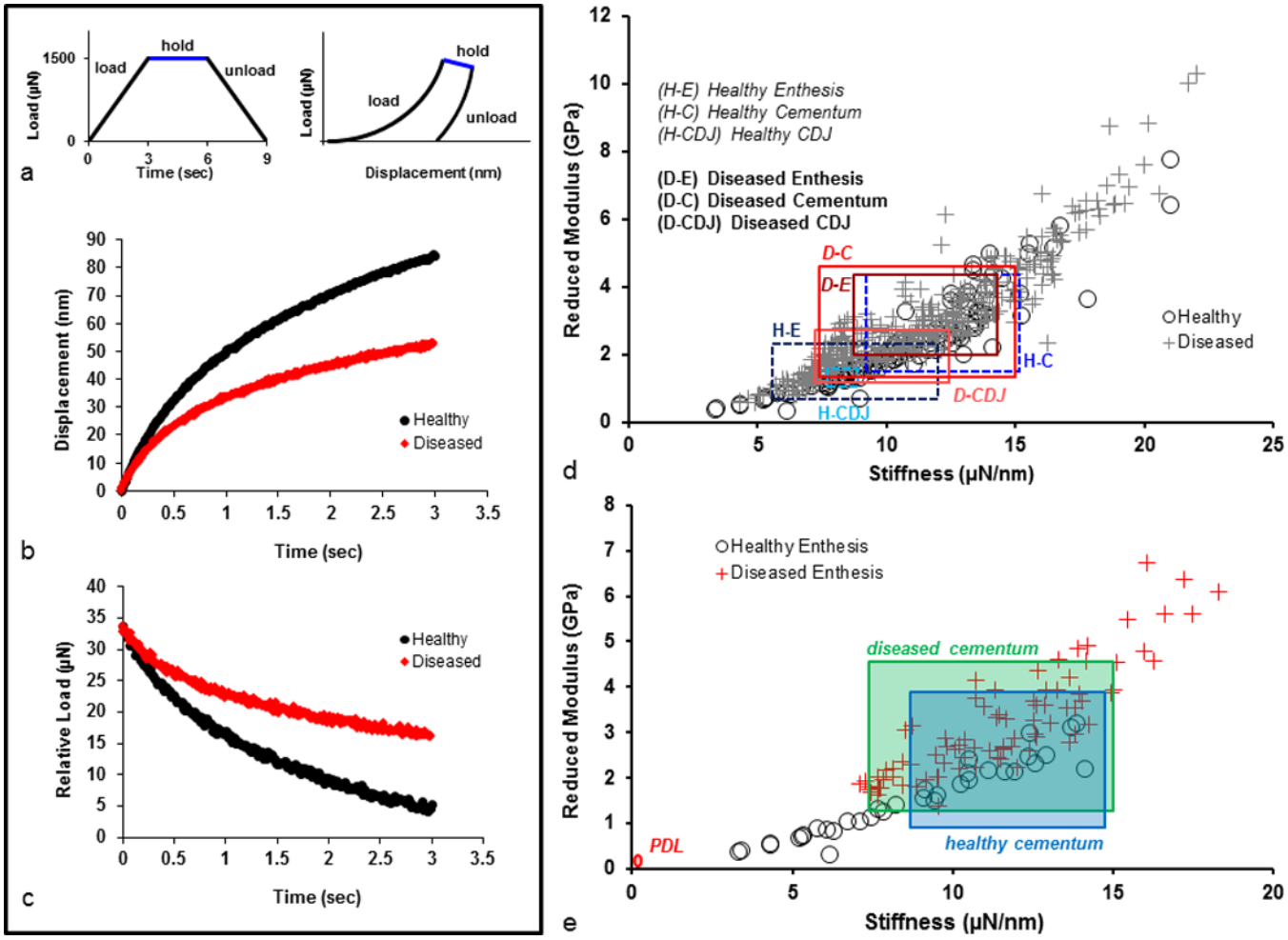

Figure 5.

A representative load-time curve includes 3 segments: load, hold, and unload (a). Each segment occurred over 3s with a maximum load at 1500 μN. The representative load-displacement profile for each corresponding segment is shown. The change in displacement (b) and load (c) over the hold segment for healthy (black) and diseased (red) specimens were examined for time related behavior. The spread of S vs. E_r illustrate one standard deviation above and below average values for specific regions in healthy and diseased specimens (d). S vs. E_r values for healthy and diseased entheses only were used to compare with representative PDL and respective cementum values (e). PDL values were taken from previous observations in our laboratory. (Enth – enthesis; Cem – cementum; CDJ – cementum-dentin junction)

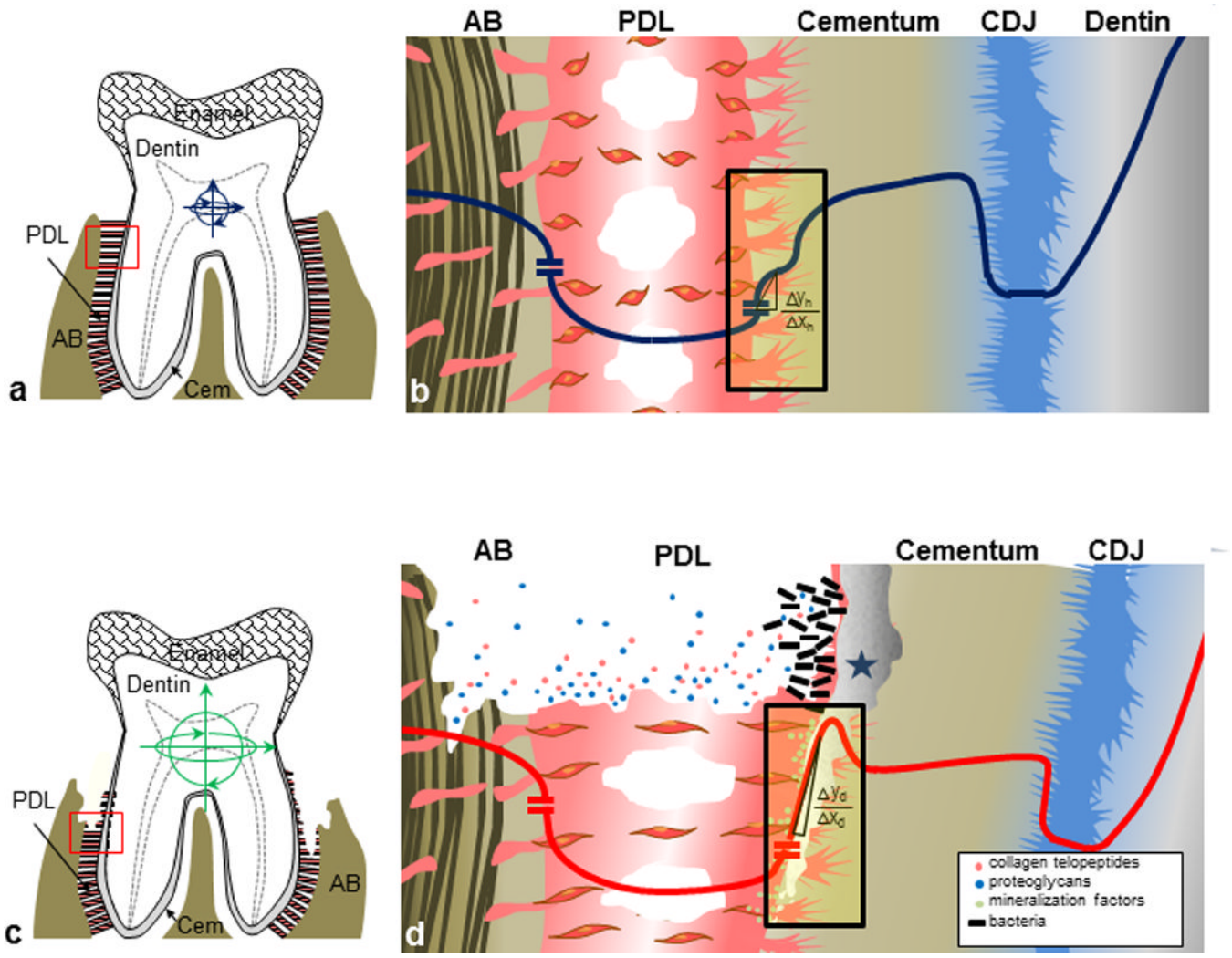

Figure 6.

(a) In a healthy tooth attachment, range of motion (blue arrows) is limited to a PDL functional space of 150–380 μm. (b) Schematic diagram of a healthy complex corresponding to the red box (a, red). The line represents elastic gradients through the PDL-bone and PDL-cementum interfaces and the cementum-dentin complex (dark blue). (c) The periodontally diseased tooth attachment process illustrating severe PDL degradation and alveolar bone resorption. Increased tooth movement can be observed (green arrows) with loss of attachment. (d) Diseased complex corresponding to the boxed inset (c, red) illustrate AB resorption and PDL degradation within PDL-space and bacterial-induced mineralization at exposed tooth root surfaces (1) shifting a ramp-like to step-like (green, $\Delta yd/\Delta xd >> \Delta yh/\Delta xh$) across the PDL-cementum interface. As a result the compromised mechanotransduction can promote the expression of mineral formation and resorption related proteins (colored circles).